Dalton Transactions

An international journal of inorganic chemistry

www.rsc.org/dalton

Volume 42 | Number 15 | 21 April 2013 | Pages 5185–5588

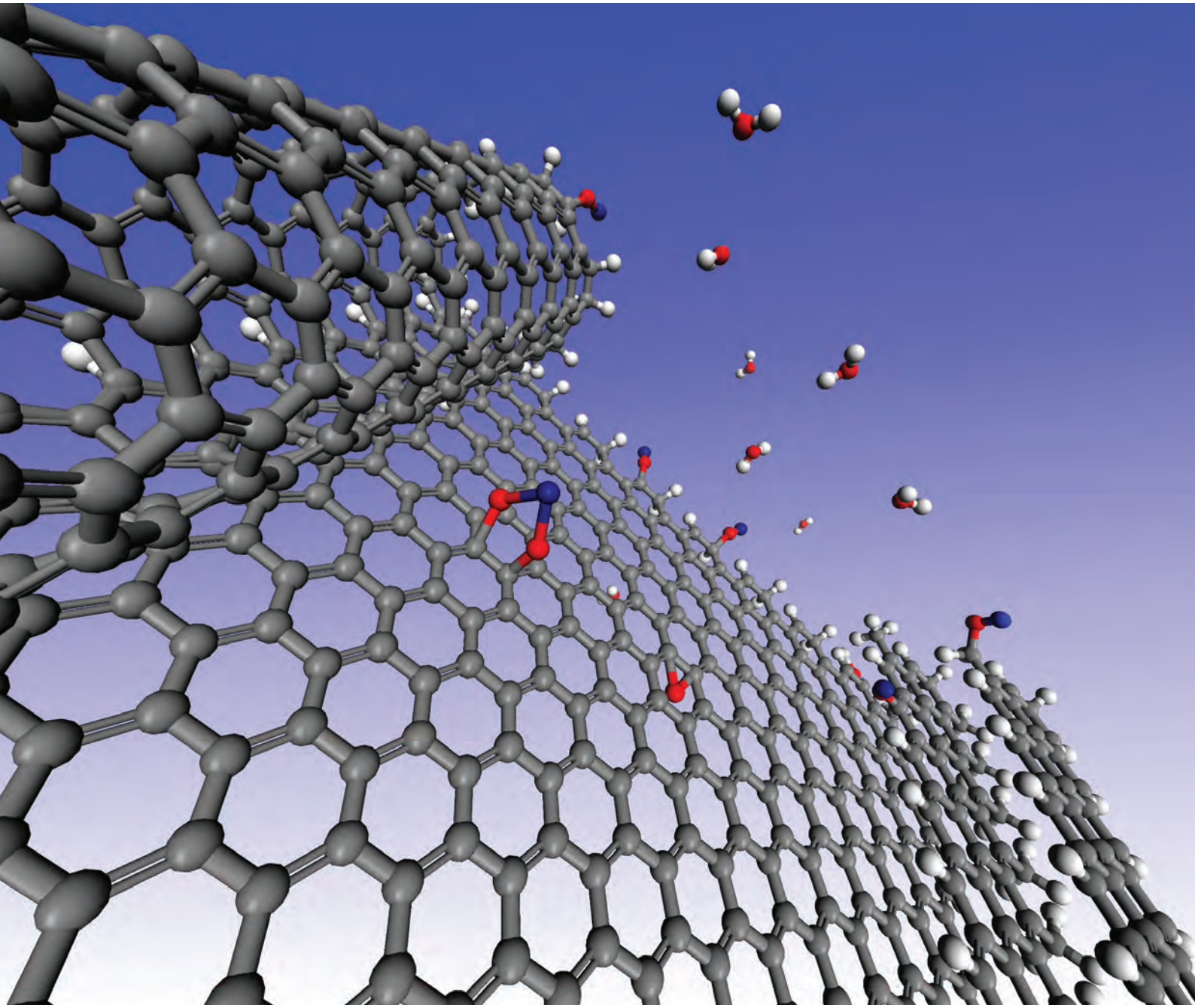

ISSN 1477-9226

RSC Publishing

COVER ARTICLE

Tan *et al.*

Comparative study of graphene oxide, activated carbon and carbon nanotubes as adsorbents for copper decontamination

Dalton Transactions

RSC Publishing

PAPER

View Article Online
View Journal | View Issue

Comparative study of graphene oxide, activated carbon and carbon nanotubes as adsorbents for copper decontamination

Cite this: *Dalton Trans.*, 2013, **42**, 5266

Xuemei Ren, Jiaxing Li, Xiaoli Tan* and Xiangke Wang

Received 11th December 2012,
Accepted 14th January 2013

DOI: 10.1039/c3dt32969k

www.rsc.org/dalton

This paper presents a comparative study of Cu(II) decontamination by three different carbonaceous materials, *i.e.*, graphene oxide, multiwalled carbon nanotubes, and activated carbon. The three carbonaceous materials were characterized by scanning electron microscopy, Fourier transform infrared spectroscopy, N_2-BET surface area analysis, and potentiometric acid–base titrations in detail. Also, Cu(II) adsorption on the three types of carbonaceous materials as a function of pH and Cu(II) ion concentration were investigated. The constant capacitance model was used to determine the appropriate surface reactions of Cu(II) adsorption on carbonaceous materials with the aid of FITEQL 4.0 software. In addition, how the surface area and the total concentration of acidic functional groups influencing the adsorption capacities of the three carbonaceous materials for Cu(II) removal were elucidated. The results have an important role in predicting the adsorption capacity of surface modified carbonaceous materials.

1. Introduction

Metal contamination is a serious and rising problem in the disposal of industrial and municipal wastewater.[1] Many papers have been published in the past few decades, confirming that the carbonaceous materials are effective adsorbents for decontamination of metal ions and their complexes.[2,3] Carbonaceous materials include a variety of stable forms ranging from naturally occurring bulk structures such as activated carbon (AC) to discrete structures such as carbon nanotubes (CNTs) and graphene. Their high sorption capacities are associated with the large specific surface area and the existence of a wide spectrum of surface functional groups.[4] AC is certainly one of the first materials applied as adsorbent and has good performance in the removal of heavy metal ions.[4,5] CNTs are relatively new efficient carbonaceous sorbents for trace pollutant decontamination due to their large specific surface area and hollow structure. Extensive efforts have led to remarkable progress in the application of CNTs for metal ion removal, which has been discussed in recent reviews.[3,6] Graphene oxide (GO), a fascinating new member of the carbon family, has been one of the worldwide hotspots of research due to its potential applications since its discovery. Its large specific surface area indicates it can be used as an efficient adsorbent.[7–10]

Different extents of aliphatic sp^3 or aromatic sp^2 hybridization of the carbon atoms in the carbonaceous materials results in different bonding and ring structures.[11] For example, AC is amorphous carbon of a structure primarily containing six-membered rings with sp^2 hybridized carbons, along with a wealth of non-aromatic five- and seven-membered rings.[11] As the 2D counterpart of naturally occurring 3D graphite, graphene is the hypothetical infinite aromatic sheet with sp^2 hybridization of the carbon atoms.[12] While, the structure of multiwalled carbon nanotubes (MWCNTs) can be rationalized as resulting from the folding of several graphene sheets (sp^2-hybridized carbon) aligned in a concentric manner.[13] This topological variation results in different interactions between the carbon substrate and a guest molecule and consequently variation in adsorption behavior. The adsorption behavior of methylene blue dye on three carbonaceous materials (GO, MWCNTs and AC) was compared.[14] The results indicated that the adsorption of methylene blue dye on GO and MWCNTs was attributed to π–π electron donor acceptor interactions and electrostatic interaction, while that on AC was due to the large surface area. Heavy metal ions are also important contaminants which can be concentrated by carbonaceous materials.[2–6] However, little effort has been made to compare the adsorptive role of carbonaceous materials for heavy metal ions and address the associated underlying mechanisms. Herein, we analyzed and compared the adsorption behaviors of different types of carbonaceous materials for metal ion

Key Laboratory of Novel Thin Film Solar Cells, Institute of Plasma Physics, Chinese Academy of Sciences, P.O. Box 1126, 230031 Hefei, P.R. China.
E-mail: tanxl@ipp.ac.cn; Fax: +86-551-5591310; Tel: +86-551-5592788

removal by coupling characterization of carbonaceous materials with quantitative analysis of the adsorption data. As an example, we chose the study of Cu(II) adsorption on three different carbonaceous materials, *i.e.*, GO, MWCNTs, and AC. In addition, the experimental data of Cu(II) adsorption on GO, MWCNTs, and AC as a function of pH were modeled by the constant capacitance model (CCM) with the aid of FITEQL 4.0 software to provide insight into the adsorption mechanism of Cu(II) on carbonaceous materials. Cu(II) is selected as a typical heavy metal ion due to its extensive environmental impact.[15] It is essential for life in trace quantities, but is toxic at high concentration levels. So, it is necessary to control the Cu(II) concentration below the permissible limits before its discharge to the environment. The aim of this work is to establish the existing similarities and differences between these materials concerning their application for the decontamination and enrichment of Cu(II) ions from aqueous solutions. The results are also used to assess whether GO is a promising substitute to CNTs and the conventional AC.

2. Material and experiments

2.1 Materials

MWCNTs were obtained from Shenzhen Bill Technology Developing Co., Ltd (Shenzhen, China). AC was purchased from Tianjin Fuchen Chemical Reagents Factory (Tianjin, China). The MWCNTs and AC were used as received without any treatment. GO was prepared from the natural flake graphite (average particle diameter of 20 mm, 99.95% purity, Qingdao Tianhe Graphite Co. Ltd, China) by using the modified Hummers method.[16] The detailed information was described in our previous studies.[8]

All the other chemicals used in the experiments were purchased from Sinopharm Chemical Reagent Co. Ltd in analytical grade. Milli-Q water (18.2 MΩ cm^{-1}) was used in the experiments. The Cu(II) stock solution was prepared by dissolving $CuCl_2$ in Milli-Q water and then diluted to 1.416×10^{-3} mol L^{-1}.

2.2 Characterization

GO, MWCNTs and AC were characterized by scanning electron microscopy (SEM), Fourier transform infrared (FTIR) spectroscopy, N_2-BET surface area analysis and potentiometric acid–base titration. The SEM images of samples were carried on a field emission scanning electron microscope (FEI Sirion 200 FEG SEM) at 5.0 kV. The FTIR measurements were mounted by using the Perkin-Elmer 100 spectrometer (America) at room temperature. The surface area was evaluated by a Micromeritics ASAP 2020 M+C accelerated surface area analyzer. The potentiometric acid–base titrations of GO, MWCNTs and AC were performed at 303 K with a Mettler Toledo DL50 titration apparatus (Switzerland) under Ar gas conditions, using NaCl as the background electrolyte and NaOH (0.04909 mol L^{-1}) as the titrant.

2.3 Batch experiments

The adsorption experiments of Cu(II) on GO, MWCNTs and AC were carried out in a series of polyethylene tubes by using the batch technique. The stock suspension of adsorbent (GO, MWCNTs or AC) and the stock solutions of Cu(II) and NaCl were added in polyethylene test tubes to achieve the desired concentrations of different components. The desired pH values (3.0–10.0) of the suspension in each tube were adjusted by adding negligible amounts of 0.1 or 0.01 mol L^{-1} NaOH or HCl. Adsorption isotherms were run by taking different concentrations of Cu(II) at fixed temperature (303 K) and pH (5.0). After the suspensions were shaken for 24 h to achieve adsorption equilibration, the solid phase was separated from the solution by a 0.45 μm membrane filter. The concentration of Cu(II) was determined by an Inductively Coupled Plasma-Atomic Emission Spectrometer (ICP-AES, Perkin-Elmer). The adsorption percentage of Cu(II) on carbonaceous materials was calculated from the difference between the initial concentration (C_0 (mol L^{-1})) and the equilibrium one (C_e (mol L^{-1})) (*i.e.*, adsorption (%) = $(C_0 - C_e)/C_0 \times 100\%$, and $C_s = (C_0 - C_e)/m_{adsorbent} \times V$, where C_s (mol g^{-1}) is the concentration of ions adsorbed on per gram of solid, V (L) is the volume of the suspension, and $m_{adsorbent}$ (g) is the mass of the adsorbents).

3. Results and discussion

3.1 Characterization of GO, MWCNTs and AC

The morphology of carbonaceous materials was studied by SEM. The results are shown in Fig. 1. It can be seen that

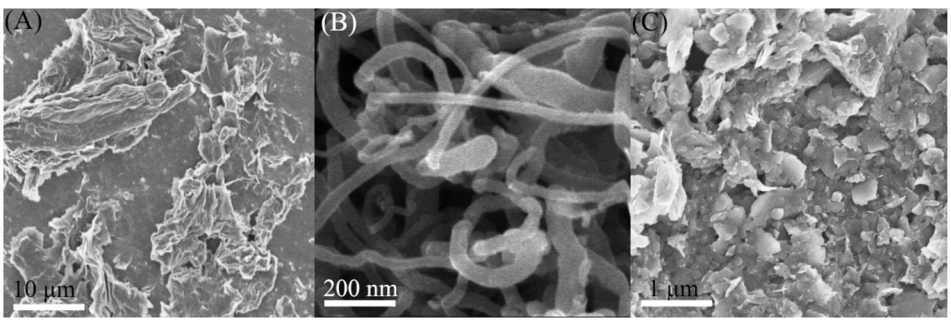

Fig. 1 SEM images of GO (A), MWCNTs (B) and AC (C).

Table 1 Physical properties of GO, MWCNTs and AC

	Specific surface area ($m^2\ g^{-1}$)	Pore volume ($cm^3\ g^{-1}$)	Average pore diameter (nm)
GO	148.34	0.091	2.44
MWCNTs	93.59	0.58	24.85
AC	28.64	0.038	5.35

carbonaceous materials have very distinct morphological features. GO has irregular edges, rough surface and lots of crumpling resulting from the scrolling of GO sheets. MWCNTs have a smooth surface and cylindrical shapes 1–10 μm long and 10–30 nm outer diameter. Further, MWCNTs are curved and entangled with each other. AC has a very rough surface and an irregular structure with cracks and crevices, confirming an amorphous structure.

The textural characteristics of GO, MWCNT and AC were characterized by N_2-BET surface area analysis. Table 1 presents the specific surface area, pore volume and average pore diameter of GO, MWCNTs and AC. The surface area is the main factor determining the physical adsorption capacity. As shown in Table 1, the surface area of GO is the highest, followed by MWCNTs, and then AC.

The major functional groups were commonly identified by using FTIR spectroscopy. The FTIR spectra of GO, MWCNTs and AC are presented in Fig. 2. All FTIR spectra of carbonaceous materials exhibit the intense absorption band assigned to O–H bond stretching, which is located at 3405 cm^{-1} for GO, 3428 cm^{-1} for MWCNTs and 3426 cm^{-1} for AC.[14,17] The peak at 1624–1625 cm^{-1} being attributed to the characteristic bands of graphite structure (sp^2 hybridized C=C) is found in all three carbonaceous materials, too.[18,19] The appearance of the peaks at 1744 cm^{-1} as well as 1423 cm^{-1} for GO and 1737 cm^{-1} as well as 1459 cm^{-1} for MWCNTs is attributed to the presence of C=O.[17,20] Addition peaks observed at 1246 cm^{-1} and 1059 cm^{-1} for GO are assigned to the presence of C–O–C and C–O, respectively.[21] According to the previous reports,[22,23] the carbonyl and carboxyl groups are located at the edges of GO, while the hydroxyl and epoxy groups are distributed mostly on the basal planes of GO. New bands at 2923 cm^{-1}, 2860 cm^{-1} and 1392 cm^{-1} found for MWCNTs are assigned to asymmetric stretching of CH_2 groups, symmetric stretching of CH_2 groups, and the disordered structure of MWCNTs, respectively.[24] Additional bands ranging from 1120 to 1049 cm^{-1} for MWCNTs are due to the presence of C–O bond.[25] The peaks at 1448 cm^{-1}, 1034 cm^{-1}, and 799 cm^{-1} as well as 695 cm^{-1} appeared in the FTIR spectrum of AC are attributed to the ring mode of the aromatic ring,[25] the stretching vibration mode of the C–H,[26] and the out of plane bending mode of the C–H or O–H groups,[27] respectively. From the FTIR spectrum analysis, it can be concluded that the spectra of carbonaceous materials present different peak distributions to each other. But all carbonaceous materials have oxygen-containing functional groups, which can provide chemical adsorption sites for heavy metal ions.

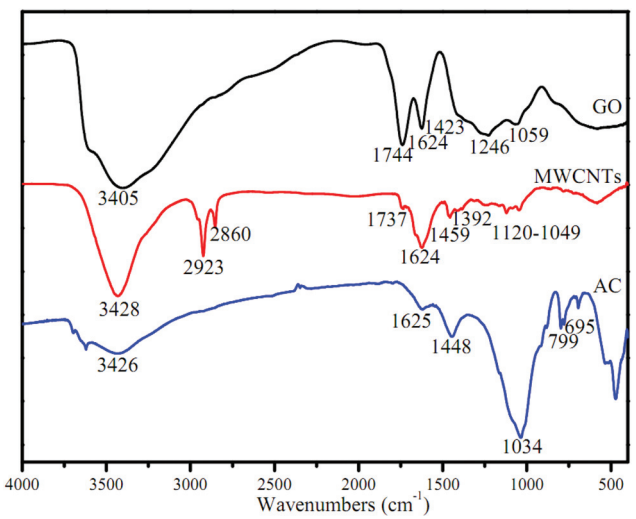

Fig. 2 FTIR spectrum curves of GO, MWCNTs and AC.

3.2 Potentiometric acid–base titration

The surfaces of carbonaceous material can be considered to be an amphoteric surface site with surface hydroxyl groups. It can either be protonated to form a positively charged surface site or deprotonated to form the negatively charged surface site. Potentiometric titration provides a measure of the sequential binding of the proton by the surface functional groups of carbonaceous materials.[28] Herein, GO, MWCNTs and AC were characterized by potentiometric titration using NaOH as the titrant.

Fig. 3(A–D) show the Gran plots for the titration data of the blank (H_2O) sample, GO, MWCNTs and AC. The Gran function (G) is expressed as:

$$\text{at acidic side: } G_a = (V_0 + V_{at} + V_b) \times 10^{-pH} \times 100, \quad (1)$$

$$\text{at alkaline side: } G_{bo} = (V_0 + V_{at} + V_b) \times 10^{-(13.8-pH)} \times 100, \quad (2)$$

where G_a and G_b are the Gran functions at the acidic and alkaline sides, respectively, V_0 (mL) is the initial solution volume, V_{at} (mL) represents the total volume of HCl added before titration to achieve pH ~ 3, V_b (mL) represents the volume of NaOH added at the different titration points. The hydroxide ions added to the suspension of carbonaceous materials are consumed by three steps reflected in the Gran plots: neutralization with excess H^+ (before V_{eb1}), interaction with the various OH^- acceptors on the surface of carbonaceous materials (between V_{eb1} and V_{eb2}), and adjustment of the pH of suspension (after V_{eb2}). The two equivalent points, V_{eb1} and V_{eb2}, are obtained from linear regression of the Gran plots as shown in Fig. 3(A–D). In fact, before V_{eb1}, the added OH^- reacts with the excess of HCl initially added into the system, so V_{eb1} can be considered as the zero titration point of carbonaceous material. It can be employed to calculate the amount of total protons. The V_{eb1} and V_{eb2} in the blank system are of almost

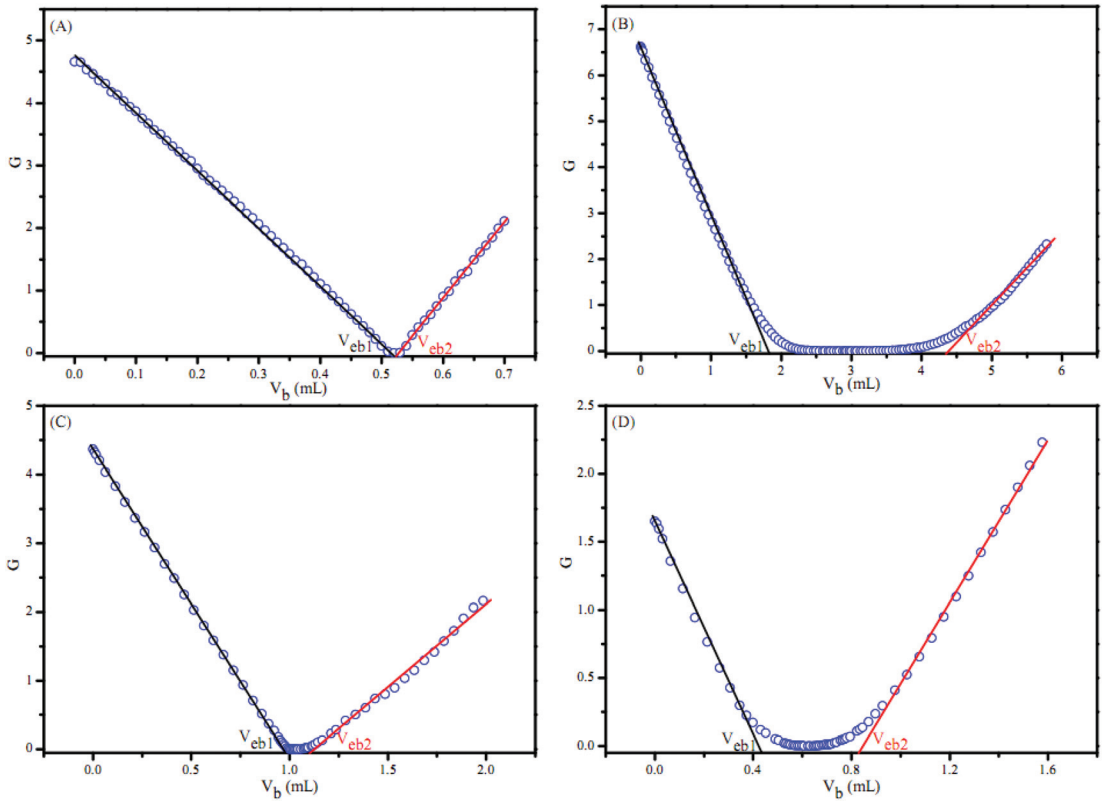

Fig. 3 Gran plots of blank (A), GO (B), MWCNTs (C) and AC (D) samples.

Table 2 Two equivalent points (V_{eb1} and V_{eb2}) obtained from linear regression of the Gran plots

	V_{eb}		
	V_{eb1}	V_{eb2}	H_s (mmol g^{-1})
GO	1.88	4.41	1.24
MWCNTs	0.98	1.10	0.061
AC	0.43	0.82	0.19

the same level, resulting from the fact that there is no buffering capacity in the blank system. However, a distinct difference between V_{eb1} and V_{eb2} is observed for the titrations of carbonaceous materials (see Table 2), indicating that the three carbonaceous materials have different buffering capacity. The added titrant firstly reacts with extra acid in solution, then reacts with the functional groups of carbonaceous materials, and finally results in the increase in total pH.

The potentiometric titration data for the blank sample and carbonaceous materials are shown in Fig. 4. TOTH, the total concentration of protons consumed in the titration process, can be calculated from the following equation:

$$\mathrm{TOTH} = \frac{-(V_b - V_{eb1})C_b}{V_0 + V_{at} + V_b}\ (\mathrm{mol\ L^{-1}}), \qquad (3)$$

where C_b represents the concentration of NaOH. Fig. 4 shows that achieving the same pH value, the amounts of OH^- consumed decrease in the order of GO > AC > MWCNTs > blank sample (H_2O), which means that the buffer capacity of GO is the highest, whereas that of MWCNTs is the lowest.

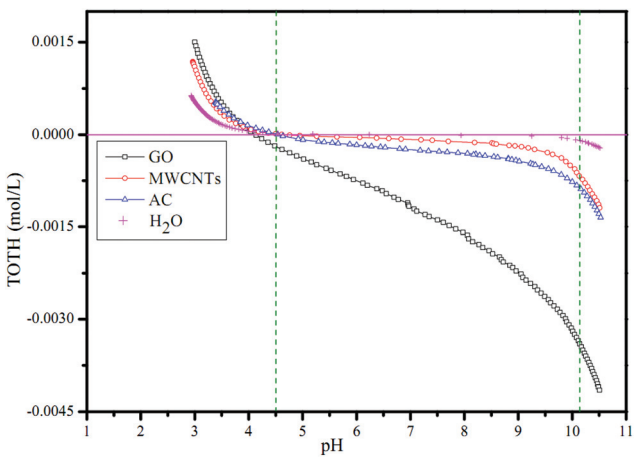

Fig. 4 TOTH curves of blank (H_2O), GO, MWCNTs and AC samples as a function of pH.

The total concentration of surface acidic groups per solid weight (H_s) calculated from the two equivalence points on the Gran plot (V_{eb1} and V_{eb2}) is defined by the following formula:[29]

$$H_s = \frac{(V_{eb2} - V_{eb1})C_b}{m_s}\ (\mathrm{mmol\ g^{-1}}). \qquad (4)$$

The results calculated from the titration curves are listed in Table 2. The total concentration of surface functional groups on GO is 1.24 mmol g^{-1}, which is 6.53 times of those on AC and 20.33 times of those on MWCNTs. GO has more functional groups reacting with OH^-, which can explain why the buffer capacity of GO is much higher than those of AC and MWCNTs.

Previous investigations reported that carbonaceous materials bear acidic characteristic surface functional groups such as carboxylic and phenolic groups.[30–32] In the present study, ≡XOH is used to represent strong acidic groups, while ≡YOH is employed to represent weak acidic groups. Both protonation and deprotonation reactions on ≡XOH are considered, while only deprotonation reaction on ≡YOH is assumed.[33] Three reactions are used to account for the acid–base chemistry of the carbonaceous materials:

$$\equiv XOH + H^+ \rightarrow \equiv XOH_2{}^+ \quad (5)$$

$$\equiv XOH \rightarrow \equiv XO^- + H^+ \quad (6)$$

$$\equiv YOH \rightarrow \equiv YO^- + H^+ \quad (7)$$

where $\equiv XOH_2{}^+$, ≡XOH and $\equiv XO^-$ represent positively charged, neutral and negatively charged strong acidic group sites on the surface of carbonaceous materials, respectively. While ≡YOH and $\equiv YO^-$ represent neutral and negatively charged weak acidic group sites on the surface of carbonaceous materials, respectively. Corresponding mass-action expressions and their intrinsic acidity constants of reactions (5)–(7) can be expressed as:

$$K_1^{int} = \frac{[\equiv XOH_2{}^+]}{[\equiv XOH][H^+]\gamma_{H^+}} \exp\left(\frac{F\psi}{RT}\right) \quad (8)$$

$$K_2^{int} = \frac{[\equiv XO^-][H^+]\gamma_{H^+}}{[\equiv XOH]} \exp\left(\frac{F\psi}{RT}\right) \quad (9)$$

$$K_3^{int} = \frac{[\equiv YO^-][H^+]\gamma_{H^+}}{[\equiv YOH]} \exp\left(\frac{F\psi}{RT}\right) \quad (10)$$

Based on CCM fitting, the distributions of surface sites on GO, AC and MWCNTs as a function of pH calculated from titration curves with the aid of the FITEQL 4.0 code are shown in Fig. 5. The relative coefficients are listed in Table 3. One can see that the distributions of surface sites on GO, AC and MWCNTs as a function of pH show a similar trend. That is the ≡YOH is the dominant species on all carbonaceous materials and its concentration decreases with increasing pH values, whereas the concentrations of $\equiv XO^-$ and $\equiv YO^-$ increase with increasing pH values. However, the total concentration of surface acidic groups and the relative ratio of ≡XOH and ≡YOH of GO, AC and MWCNTs are not the same as each other, resulting in different acid–base chemistry of the carbonaceous materials and thus different adsorption properties of the carbonaceous materials.

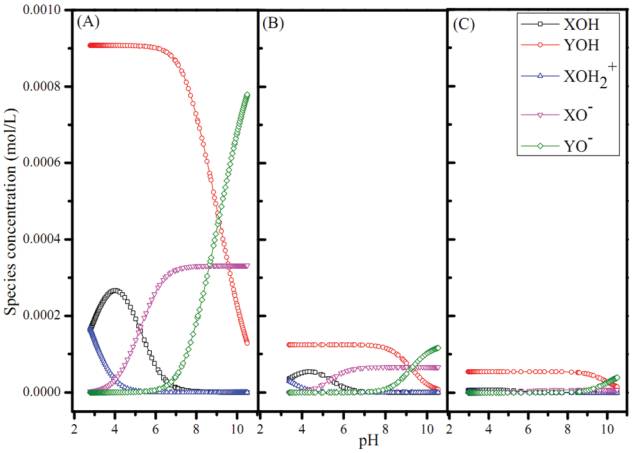

Fig. 5 Surface site concentrations of GO (A), AC (B) and MWCNTs (C) as a function of pH simulated by CCM with the aid of FITEQL 4.0 code.

Table 3 log *K* values obtained by CCM3 with the aid of FITEQL 4.0

	log K^{int}		
	GO	AC	MWCNTs
Acid–base reactions			
$\equiv XOH + H^+ \rightarrow \equiv XOH_2{}^+$	3.10	3.41	2.48
$\equiv XOH \rightarrow \equiv XO^- + H^+$	−4.92	−5.30	−5.60
$\equiv YOH \rightarrow \equiv YO^- + H^+$	−7.63	−8.95	−9.82
Surface complexation reactions			
$\equiv XOH + Cu^{2+} \rightarrow \equiv XOHCu^{2+}$	2.80	0.82	
$\equiv XOH + Cu^{2+} \rightarrow \equiv XOCu^+ + H^+$	−1.88	−2.06	
$\equiv YOH + Cu^{2+} \rightarrow \equiv YOCu^+ + H^+$	−3.73	−2.77	−4.00
$2\equiv YOH + Cu^{2+} \rightarrow \equiv (YO)_2Cu + 2H^+$	−5.07	−6.56	−5.21

3.3 Adsorption studies

The adsorption of aqueous metal species on carbonaceous material is affected by surface charge of adsorbent and speciation of metal ions in solution, which leads to a dependence of the amount adsorbed on the point of zero charge (pH_{PZC}) of adsorbent and experimental conditions. The adsorption studies of Cu(II) on carbonaceous materials were performed by investigating the effect of pH and Cu(II) concentration.

3.3.1 pH effect. The pH of the solution influences the surface chemical properties of adsorbent and the solution chemistry of the adsorbate in the aqueous solution.[34] At the low acidic pH medium, the functional groups on the adsorbent surface are protonated to form the positive surface charge, while free metal ions are present in solution. The electrostatic repulsion between the positively charged adsorbent surface and the free metal ions as well as the competition between H^+ and free metal ions for the limited active surface sites leads to a low adsorption percentage. At alkaline pH medium, the functional groups on the adsorbent surface are deprotonated to form the negative surface charge, while part of the metal ions may form precipitates as their hydroxides. The electrostatic attraction, inner-sphere surface complexation and surface precipitation increase the adsorption

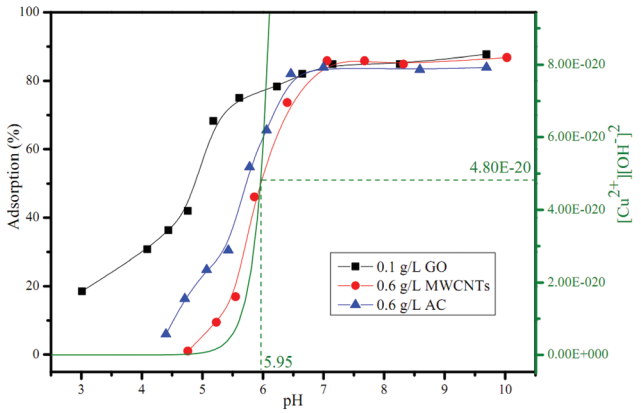

Fig. 6 pH dependent adsorption of Cu(II) on GO, MWCNTs and AC. $C_{(Cu(II))initial}$ = 2.36 × 10^{-4} mol L^{-1}, I = 0.01 mol L^{-1} NaCl, T = 303 K.

performance. Thereby, the adsorption of metal ions on solid particles may alter at various pH values.

Fig. 6 presents the adsorption of Cu(II) ions on GO, MWCNTs and AC as a function of pH. The adsorption percentages of Cu(II), at a given initial Cu(II) concentration (C_0 = 2.36 × 10^{-4} mol L^{-1}), on all investigated carbonaceous adsorbents increase as pH increases, which is consistent with previous reports with respect to heavy metal ion adsorption to various carbonaceous adsorbents such as GO,[7] AC,[26] and CNTs.[35] The affinity of Cu(II) ions towards the carbonaceous materials is: GO > AC > CNTs. More than 75% of Cu(II) ions are removed from aqueous solution onto GO at pH 5.5, while only 36% of Cu(II) ions are removed from solution onto AC at the similar pH value.

pH_{PZC} controls the Coulomb interactions between the surface of carbonaceous materials and the aqueous metal ions, the stability of colloidal suspensions, and thereby the metal ion uptake.[36] The pH_{PZC} of carbonaceous materials depends on surface acidic functional groups.[37,38] The higher concentration of surface acidic functional groups, the lower pH_{PZC} value of carbonaceous materials. Based on our results of potentiometric acid–base titrations, it can be deduced that the pH_{PZC} values of carbonaceous materials decrease in the order of pH_{PZC}(GO) < pH_{PZC}(AC) < pH_{PZC}(MWCNTs). This is in agreement with a previous report, which suggested that a much lower value of pH_{PZC} of carbonaceous materials is directly associated to the greater amount of surface acidic functional groups.[39] The carbonaceous surface is positively charged at pH values below the pH_{PZC} and negatively charged at pH values above the pH_{PZC}.[40] The low pH_{PZC} is conducive to the retention of Cu(II) ions. GO has the lowest pH_{PZC} and the maximum efficiency in Cu(II) decontamination.

The solubility product constant of $Cu(OH)_{2(s)}$ is 4.8 × 10^{-20}, and the precipitation curve of Cu(II) at the concentration of 2.36 × 10^{-4} mol L^{-1} is also shown in Fig. 6. It is clear that Cu(II) ions begin to form precipitation at pH 5.95 if no Cu(II) is adsorbed. In the presence of carbonaceous materials, more than 60% Cu(II) are adsorbed at pH 5.95. In theory, the adsorption of Cu(II) on carbonaceous materials at pH < 5.95 is not due to the surface precipitation of $Cu(OH)_{2(s)}$. While, copper hydroxide precipitates are formed under alkaline conditions (pH > 7.0). Meanwhile, the surfaces of the three carbonaceous adsorbents are negatively charged at pH > 7.0, and the adsorption of positively charged Cu(II) species (Cu^{2+} and $Cu(OH)^+$) becomes more favorable. Thereby, Cu(II) can be almost completely removed by the three carbonaceous adsorbents due to the simultaneous precipitation of $Cu(OH)_2^0$ and the adsorption of Cu^{2+} and $Cu(OH)^+$ at pH 7.0–10.0. In order to eliminate the influence of precipitation on Cu(II) uptake from solution, the adsorption isotherms of Cu(II) on the three carbonaceous adsorbents are investigated at pH 5.0.

At pH < 5.95, Cu(II) adsorption data are fitted using the CCM with the aid of FITEQL 4.0 software (Fig. 7). According to

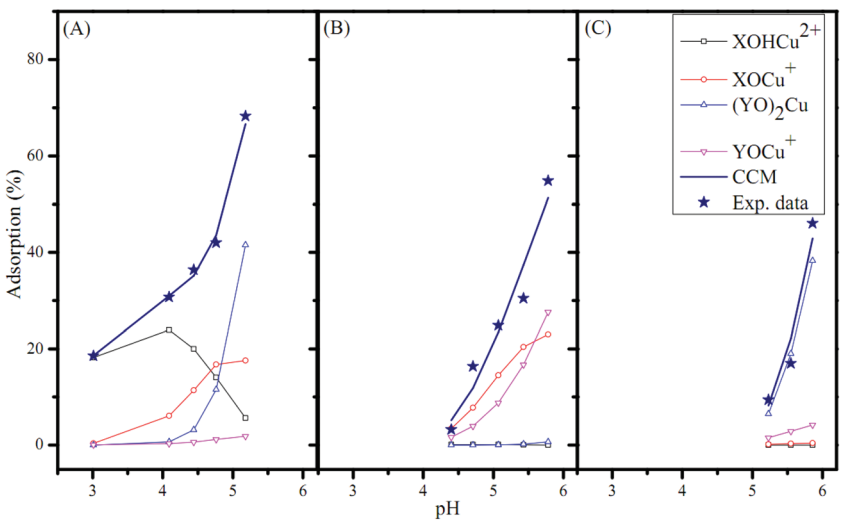

Fig. 7 Surface complex speciation repartition diagram of Cu(II) adsorption on GO (0.1 g L^{-1}, A), AC (0.6 g L^{-1}, B) and MWCNTs (0.6 g L^{-1}, C) as a function of pH (pH < 5.95). Point: experimental data; solid line: CCM simulation. $C_{(Cu(II))initial}$ = 2.36 × 10^{-4} mol L^{-1}, I = 0.01 mol L^{-1} NaCl, T = 303 K.

the analysis of the distribution of aqueous Cu(II) species reported by Wu and coworkers,[41] at pH < 5.95, only Cu^{2+} species is considered in developing the set of surface reactions between Cu(II) and carbonaceous materials. At the same time, considering the distribution of surface complex sites on carbonaceous materials, ≡XOH, $\equiv XO^-$ and ≡YOH exist on carbonaceous material surfaces at pH < 5.95. Possible reactions for Cu(II) retention on carbonaceous materials are:

$$\equiv XOH + Cu^{2+} \rightarrow \equiv XOHCu^{2+} \quad (11)$$

$$\equiv XOH + Cu^{2+} \rightarrow \equiv XOCu^{+} + H^{+} \quad (12)$$

$$\equiv YOH + Cu^{2+} \rightarrow \equiv YOCu^{+} + H^{+} \quad (13)$$

$$2\equiv YOH + Cu^{2+} \rightarrow \equiv (YO)_2Cu + 2H^{+} \quad (14)$$

The experimental data, fit curves and surface species distributions of Cu(II) adsorbed on carbonaceous materials are shown in Fig. 7. The optimized constants are listed in Table 3. As can be seen from Fig. 7, the adsorption of Cu(II) on GO can occur at pH = 3.0, and $\equiv XOHCu^{2+}$, $\equiv XOCu^{+}$ and $\equiv (YO)_2Cu$ complexes are the main species. $\equiv XOHCu^{2+}$ is the dominant surface species at low pH values. It increases with increasing pH values, reaches the maximum and then decreases. While $\equiv XOCu^{+}$ and $\equiv (YO)_2Cu$ increase with increasing pH values, and the latter becomes the dominant surface species with further increasing pH values. The adsorption of Cu(II) on AC occurs at pH > 4.0, and $\equiv XOCu^{+}$ and $\equiv YOCu^{+}$ complexes are the main species. Both of them increase with increasing pH values. The adsorption of Cu(II) on MWCNTs occurs at pH > 5.0, and $\equiv YOCu^{+}$ and $\equiv (YO)_2Cu$ complexes are the main species. As discussed above, GO has a stronger multisite adsorption behavior than AC and MWCNTs, which results in a wider adsorption *vs.* pH profile (Fig. 6).[42] The high abundance of ≡YOH surface site relative to ≡XOH on MWCNTs (Fig. 5) explains the predominant role of $\equiv YOCu^{+}$ and $\equiv (YO)_2Cu$ in the pH range of 5.0–5.9.

3.3.2 Adsorption isotherms. The partitioning of Cu(II) between the aqueous phase and the three carbonaceous adsorbents at pH 5.0 as a function of Cu(II) concentrations is shown in Fig. 8. GO presents the highest adsorption capacity, followed by AC and MWCNTs. For interpretation of the adsorption data, the Langmuir[43] and Freundlich[44] isotherm models are used.

The Langmuir isotherm is present as:

$$C_s = C_{smax}\frac{K_L C_e}{1 + K_L C_e} \quad (15)$$

The Freundlich equation is given as:

$$C_s = K_F C_e^n \quad (16)$$

where C_{smax} is the maximum amount of Cu(II) per unit weight of carbonaceous adsorbents to form a complete monolayer coverage on the surface, and K_L is the Langmuir constant. K_F and n are Freundlich constants.

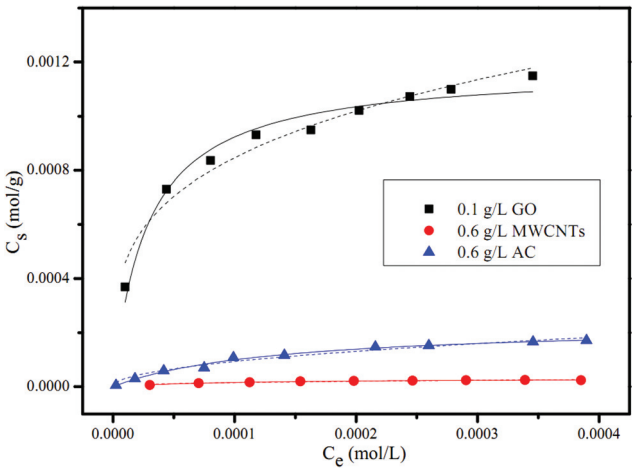

Fig. 8 Adsorption isotherms of Cu(II) on GO, MWCNTs and AC. pH = 5.0, I = 0.01 mol L^{-1} NaCl, T = 303 K. Symbols denote experimental data, solid lines represent the model fitting of Langmuir equation, and dash lines represent the model fitting of Freundlich equation.

Table 4 Parameters for the calculation using Langmuir and Freundlich models

Model	Parameter	GO	MWCNTs	AC
Langmuir isotherm fit	C_{smax} (mol g^{-1})	1.18×10^{-3}	3.19×10^{-5}	2.31×10^{-4}
	K_L (L mol^{-1})	3.62×10^{4}	9.54×10^{3}	7.59×10^{3}
	R^2	0.967	0.992	0.989
Freundlich isotherm fit	N	0.27	0.42	0.49
	K_F (mol^{1-n} L^n g^{-1})	0.0099	6.92	0.0085
	R^2	0.962	0.939	0.968

The Langmuir and Freundlich isotherm parameters determined from adsorption isotherms of Cu(II) on the three carbonaceous adsorbents at pH 5.0 are listed in Table 4. From the correlation coefficients, one can see that the Langmuir model fits the experimental data better than the Freundlich model. According to the Langmuir model simulation, the maximum adsorption capacities (C_{smax}) of Cu(II) are 1.18×10^{-3} mol g^{-1} for GO, 3.19×10^{-5} mol g^{-1} for MWCNTs, and 2.31×10^{-4} mol g^{-1} for AC. It can be seen that GO has the better performance in copper decontamination than AC and MWCNTs.

3.4 Relationship between C_{smax} and H_s

Even though the surface area of AC is less than that of MWCNTs, the adsorption capacity of AC is larger than that of MWCNTs, which could be explained by the fact that the AC possesses greater surface total acidities than the MWCNTs as shown in Table 2. It is further supported in Fig. 9(A) and 9(B), which show that C_{smax} is linearly dependent on H_s (the related coefficient is 0.992) and that C_{smax} of carbonaceous materials increases with increasing H_s normalized by the BET surface area, respectively. One can see that Cu(II) adsorption on carbonaceous adsorbents is dependent on the total concentration of surface acidic groups on the carbonaceous adsorbents rather than the available total surface area. This result is consistent with previous studies of Ni^{2+} retention on CNTs and granular AC.[20] Similar findings have also been reported in the

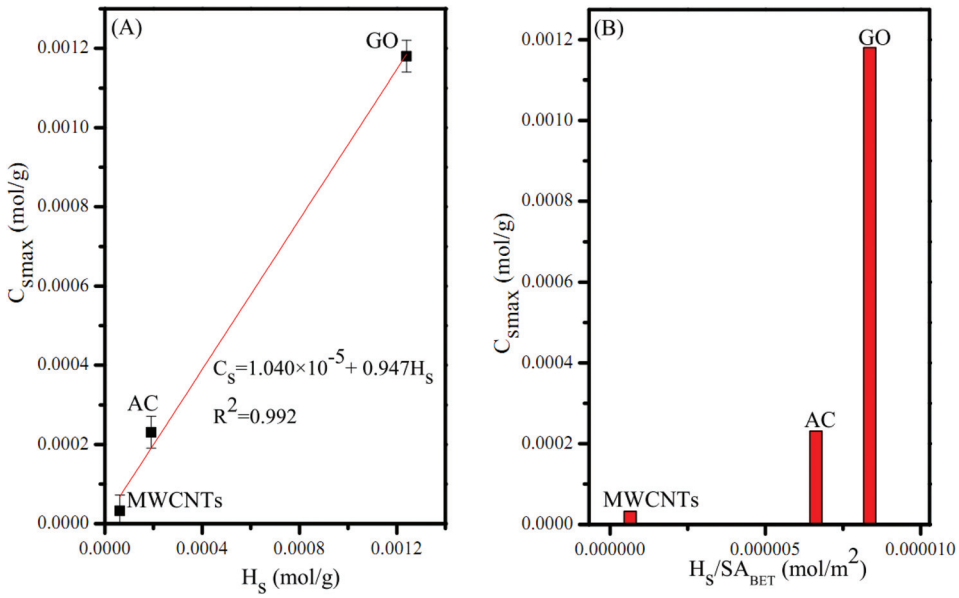

Fig. 9 (A) Relationship between C_{smax} and H_s; and (B) relationship between C_{smax} and H_s normalized by the BET surface area.

literature for the adsorption of Zn(II) onto AC[45] and for the adsorption of Pb(II) onto acidified MWCNTs.[46]

The reasons for the adsorption of different amounts of Cu(II) ions on carbonaceous materials may include the following: (1) Cu(II) speciation in solution, (2) surface heterogeneity, (3) accessibility of species to the porous structure, and (4) adsorbate–adsorbent interactions.[47] Our study shows that speciation in solution and adsorbate–adsorbent interaction are the major factors controlling the adsorption of Cu(II) on carbonaceous materials across all the pH values, while adsorbate–adsorbent interaction is the major factor at acidic pH. This is in agreement with Xiao and Thomas' report,[47] where the adsorption of metal ions on a series of carbons was found to be related to the type and concentration of surface functional groups rather than differences in the porous structure. Based on our results of CCM fitting, the adsorption of Cu^{2+} on acidic functional group sites of carbonaceous materials mainly involves three species of $\equiv XOHCu^{2+}$, $\equiv XOCu^{+}$ and $\equiv YOCu^{+}$ for GO, two species of $\equiv XOCu^{+}$ and $\equiv YOCu^{+}$ for AC, and two species of $\equiv YOCu^{+}$ and $\equiv(YO)_2Cu$ for MWCNTs at pH < 5.95.

4. Conclusions

Adsorption behaviors of Cu(II) onto three carbonaceous materials (GO, MWCNTs and AC) differing in surface area and the total concentration of acidic groups were compared. Under acidic conditions, the GO has the highest adsorption efficiency, followed by AC, and then MWCNTs, suggesting that GO is a promising material for the removal of Cu(II) ions from aqueous solutions in acidic wastewater treatment. Based on the results of CCM fitting, the species of Cu(II) present as $\equiv XOHCu^{2+}$, $\equiv XOCu^{+}$ and $\equiv YOCu^{+}$ on GO, as $\equiv XOCu^{+}$ and $\equiv YOCu^{+}$ on AC, and as $\equiv YOCu^{+}$ and $\equiv(YO)_2Cu$ on MWCNTs at pH < 5.95. The maximum adsorption capacities are 1.18 × 10^{-3} mol g^{-1} for GO, 2.31 × 10^{-4} mol g^{-1} for AC and 3.19 × 10^{-5} mol g^{-1} for MWCNTs, which are linearly dependent on the total concentration of surface acidic groups. This important observation may have an implication in predicting adsorption capacities of other carbonaceous adsorbents.

Acknowledgements

Financial supports from 973 project of MOST (2011CB933700) and National Natural Science Foundation of China (21071147; 91126020; 21077107; and 21225730) are acknowledged.

References

1 J. García-Martín, R. López-Garzón, M. L. Godino-Salido, M. D. Gutiérrez-Valero, P. Arranz-Mascarós, R. Cuesta and F. Carrasco-Marín, *Langmuir*, 2005, **21**, 6908–6914.
2 K. Pyrzyńska and M. Bystrzejewski, *Colloids Surf., A*, 2010, **362**, 102–109.
3 G. P. Rao, C. Lu and F. Su, *Sep. Purif. Technol.*, 2007, **58**, 224–231.
4 K. Pyrzynska, *Microchim. Acta*, 2010, **169**, 7–13.
5 J. Rivera-Utrilla, M. Sánchez-Polo, V. Gómez-Serrano, P. M. Álvarez, M. C. M. Alvim-Ferraz and J. M. Dias, *J. Hazard. Mater.*, 2011, **187**, 1–23.
6 X. M. Ren, C. L. Chen, M. Nagatsu and X. K. Wang, *Chem. Eng. J.*, 2011, **170**, 395–410.
7 G. X. Zhao, J. X. Li, X. M. Ren, C. L. Chen and X. K. Wang, *Environ. Sci. Technol.*, 2011, **45**, 10454–10462.

8 G. X. Zhao, X. M. Ren, X. Gao, X. L. Tan, J. X. Li, C. L. Chen, Y. Y. Huang and X. K. Wang, *Dalton Trans.*, 2011, **40**, 10945–10952.
9 Y. B. Sun, Q. Wang, C. L. Chen, X. L. Tan and X. K. Wang, *Environ. Sci. Technol.*, 2012, **46**, 6020–6027.
10 G. X. Zhao, L. Jiang, Y. D. He, J. X. Li, H. L. Dong, X. K. Wang and W. P. Hu, *Adv. Mater.*, 2011, **23**, 3959–3963.
11 J. W. Jiang, N. J. Wagner and S. I. Sandler, *Phys. Chem. Chem. Phys.*, 2004, **6**, 4440–4444.
12 S. Niyogi, E. Bekyarova, M. E. Itkis, J. L. McWilliams, M. A. Hamon and R. C. Haddon, *J. Am. Chem. Soc.*, 2006, **128**, 7720–7721.
13 I. A. A. C. Esteves, F. J. A. L. Cruz, E. A. Müller, S. Agnihotri and J. P. B. Mota, *Carbon*, 2009, **47**, 948–956.
14 Y. Li, Q. Du, T. Liu, X. Peng, J. Wang, J. Sun, Y. Wang, S. Wu, Z. Wang, Y. Xia and L. Xia, *Chem. Eng. Res. Des.*, 2013, **91**, 361–368.
15 X. Ren, S. Yang, X. Tan, C. Chen, G. Sheng and X. Wang, *J. Hazard. Mater.*, 2012, **237–238**, 199–208.
16 M. Hirata, T. Gotou, S. Horiuchi, M. Fujiwara and M. Ohba, *Carbon*, 2004, **42**, 2929–2937.
17 A. Pulido, P. Concepción, M. Boronat, C. Botas, P. Alvarez, R. Menendez and A. Corma, *J. Mater. Chem.*, 2012, **22**, 51–56.
18 P. Wu, Y. D. Qian, P. Du, H. Zhang and C. X. Cai, *J. Mater. Chem.*, 2012, **22**, 6402–6412.
19 D. D. Shao, J. Hu and X. K. Wang, *Plasma Processes Polym.*, 2010, **7**, 977–985.
20 C. Y. Lu, C. Liu and G. P. Rao, *J. Hazard. Mater.*, 2008, **151**, 239–246.
21 S. Chandra, P. Das, S. Bag, R. Bhar and P. Pramanik, *Mater. Sci. Eng., B*, 2012, **177**, 855–861.
22 D. R. Dreyer, S. Park, C. W. Bielawski and R. S. Ruoff, *Chem. Soc. Rev.*, 2010, **39**, 228–240.
23 M. Fang, K. G. Wang, H. B. Lu, Y. L. Yang and S. Nutt, *J. Mater. Chem.*, 2009, **19**, 7098–7105.
24 G. D. Vuković, A. D. Marinković, M. Čolić, M. Đ. Ristić, R. Aleksić, A. A. Perić-Grujić and P. S. Uskoković, *Chem. Eng. J.*, 2010, **157**, 238–248.
25 F. M. Machado, C. P. Bergmann, T. H. M. Fernandes, E. C. Lima, B. Royer, T. Calvete and S. B. Fagan, *J. Hazard. Mater.*, 2011, **192**, 1122–1131.
26 L. Wang, J. Zhang, R. Zhao, Y. Li, C. Li and C. L. Zhang, *Bioresour. Technol.*, 2010, **101**, 5808–5814.
27 Q. S. Liu, T. Zheng, P. Wang and L. Guo, *Ind. Crops Prod.*, 2010, **31**, 233–238.
28 R. X. Liu, X. M. Liu, H. X. Tang and Y. B. Su, *J. Colloid Interface Sci.*, 2001, **239**, 475–482.
29 N. Frini-Srasra and E. Srasra, *Surf. Eng. Appl. Electrochem.*, 2008, **44**, 401–409.
30 I. I. Salame and T. J. Bandosz, *Ind. Eng. Chem. Res.*, 2000, **39**, 301–306.
31 G. C. Chen, X. Q. Shan, Y. S. Wang, Z. G. Pei, X. E. Shen, B. Wen and G. Owens, *Environ. Sci. Technol.*, 2008, **42**, 8297–8302.
32 G. D. Sheng, D. D. Shao, X. M. Ren, X. Q. Wang, J. X. Li, Y. X. Chen and X. K. Wang, *J. Hazard. Mater.*, 2010, **178**, 505–516.
33 Z. J. Guo, J. Xu, K. L. Shi, Y. Q. Tang, W. S. Wu and Z. Y. Tao, *Colloids Surf., A*, 2009, **339**, 126–133.
34 A. Schierz and H. Zänker, *Environ. Pollut.*, 2009, **157**, 1088–1094.
35 C. L. Chen, J. Hu, D. D. Shao, J. X. Li and X. K. Wang, *J. Hazard. Mater.*, 2009, **164**, 923–928.
36 M. A. Alvarez-Merino, M. A. Fontecha-Camara, M. V. Lopez-Ramon and C. Moreno-Castilla, *Carbon*, 2008, **46**, 778–787.
37 D. Borah, S. Satokawa, S. Kato and T. Kojima, *J. Hazard. Mater.*, 2009, **162**, 1269–1277.
38 D. Borah, S. Satokawa, S. Kato and T. Kojima, *J. Colloid Interface Sci.*, 2008, **319**, 53–62.
39 M. A. A. Zaini, R. Okayama and M. Machida, *J. Hazard. Mater.*, 2009, **170**, 1119–1124.
40 D. Borah, S. Satokawa, S. Kato and T. Kojima, *Appl. Surf. Sci.*, 2008, **254**, 3049–3056.
41 X. L. Wu, D. L. Zhao and S. T. Yan, *Desalination*, 2011, **269**, 84–91.
42 J. Hizal and R. Apak, *Appl. Clay Sci.*, 2006, **32**, 232–244.
43 I. Langmuir, *J. Am. Chem. Soc.*, 1918, **40**, 1361–1403.
44 H. Freundlich, *Z. Phys. Chem.*, 1906, **57**, 385–470.
45 R. L. Ramos, L. A. B. Jacome, J. M. Barron, L. F. Rubio and R. M. G. Coronado, *J. Hazard. Mater.*, 2002, **90**, 27–38.
46 H. J. Wang, A. L. Zhou, F. Peng, H. Yu and J. Yang, *J. Colloid Interface Sci.*, 2007, **316**, 277–283.
47 B. Xiao and K. M. Thomas, *Langmuir*, 2005, **21**, 3892–3902.

